Published in final edited form as:

Oncogene. 2019 August ; 38(35): 6241–6255. doi:10.1038/s41388-019-0873-8.

EGR1 Regulates Angiogenic and Osteoclastogenic Factors in Prostate Cancer and Promotes Metastasis

Lechen Li, M.D.[2], **Amir H Ameri, B.S**[1], **Simeng Wang, M.S.**[1], **Keith H Jansson, Ph.D.**[1], **Orla M Casey, Ph.D.**[1], **Qi Yang, Ph.D**[1], **Michael L Beshiri, Ph.D**[1], **Lei Fang, Ph.D**[1], **Ross G Lake, M.S.**[1], **Supreet Agarwal, Ph.D**[1], **Aian N Alilin, B.S.**[1], **Wanhai Xu, M.D. Ph.D**[2], **JuanJuan Yin, M.D. & Ph.D**[1], **Kathleen Kelly, Ph.D.**[1]

[1]Laboratory of Genitourinary Cancer Pathogenesis, CCR, National Cancer Institute, Bethesda, MD USA

[2]Department of Urology, The Fourth Hospital of Harbin Medical University, Harbin Heilongjiang, China

Abstract

Early growth response-1 (*EGR1)* is a transcription factor correlated with prostate cancer (PC) progression in a variety of contexts. For example, *EGR1* levels increase in response to suppressed androgen receptor signaling or loss of the tumor suppressor, *PTEN. EGR1* has been shown to regulate genes influencing proliferation, apoptosis, immune cell activation, and matrix degradation, among others. Despite this, the impact of *EGR1* on PC metastatic colonization is unclear. We demonstrate using a PC model (DU145/RasB1) of bone and brain metastasis that *EGR1* expression regulates angiogenic and osteoclastogenic properties of metastases. We have shown previously that FN14 (TNFRSF12A) and downstream NF-κB signaling is required for metastasis in this model. Here we demonstrate that FN14 ligation also leads to NF-κB-independent, MEK-dependent *EGR1* expression. *EGR1*-depletion in DU145/RasB1 cells reduced both the number and size of metastases but did not affect primary tumor growth. Decreased *EGR1* expression led to reduced blood vessel density in brain and bone metastases as well as decreased osteolytic bone lesion area and reduced numbers of osteoclasts at the bone-tumor interface. TWEAK (TNFSF12) induced several *EGR1*-dependent angiogenic and osteoclastogenic factors (e.g. PDGFA, TGFB1, SPP1, IL6, IL8, and TGFA, among others). Consistent with this, in clinical samples of PC, the level of several genes encoding angiogenic/osteoclastogenic pathway effectors correlated with *EGR1* levels. Thus, we show here that *EGR1* has a direct effect on prostate cancer metastases. EGR1 regulates angiogenic and osteoclastogenic factors, informing the underlying signaling networks that impact autonomous and microenvironmental mechanisms of cancer metastases.

Corresponding authors: 1. Wanhai Xu, 37 Yiyuan St, Department of Urology, the Fourth Hospital of Harbin Medical University, Harbin, Heilongjiang Province, China, 150001, xuwanhai@163.com, +86-133-1360-2566(phone), +86-0451-8593-9377 (FAX); 2. JuanJuan Yin, 37 Convent Drive, Building 37 Room 1066, Bethesda, MD 20892, yinjuan@mail.nih.gov, 301-594-1532(phone), 240-541-4503 (FAX); 3. Kathleen Kelly, 37 Convent Drive, Building 37 Room 1068, Bethesda, MD 20892, kellyka@mail.nih.gov, 240-760-6827(phone), 240-541-4503 (FAX).

Conflict of interest

The authors declare no conflict of interest.

Keywords

prostate cancer; *EGR1*; bone metastasis; brain metastasis; FN14; angiogenesis; osteoclastogenesis

Introduction:

EGR1 is an early response gene that is involved in growth, differentiation, apoptosis, neurite outgrowth and wound healing. As a transcription factor, *EGR1* has highly conserved DNA-binding domain composed of three zinc fingers that bind to the GC-rich consensus sequence GCG (G/T) GGGCG. *EGR1* is induced by cytokines, growth factors and stress signals such as radiation, injury or mechanical stress (1). Although *EGR1* has significant tumor suppressor properties in many types of cancer (2-4), emerging evidence indicates that *EGR1* is a tumor promoter in prostate cancer. It has been reported that silencing *EGR1* impairs the progression from prostatic intraepithelial neoplasia to adenocarcinoma in the cryptdin-2-T-antigen (CR2-T-Ag) and transgenic adenocarcinoma of the mouse prostate (TRAMP) mouse model (5). In addition, using *in situ* hybridization to analyze 96 prostate specimens, Manal and colleagues demonstrated that quantified *EGR1* mRNA levels positively correlated with prostate cancer Gleason grade (6). Nevertheless, a role for *EGR1* in prostate cancer metastasis has not been established.

Elevated *EGR1* levels are associated with prostate cancer progression. For example, EGR1 expression and activity occur following experimental *Pten* loss (7). *PTEN* deletion occurs in about 20% of primary and 40% of metastatic clinical PC (8). In addition, *EGR1* expression is increased with castration (7), and overexpressing *EGR1* promotes LNCaP tumor growth in castrated nude mice (9). *EGR1* co-immunoprecipitates with AR and promotes AR-dependent transcription of PSA in prostate cancer cells (10), suggesting that EGR1 acts through an AR-dependent mechanism in promoting castration resistance. Importantly, however, EGR1 regulates various AR independent properties associated with advanced PC as well. Forced *EGR1* expression in AR positive and negative prostate cancer cell lines increased various proteins which are associated with invasive activity (hPAR, HYAL-1, HPSE, MMP9) (1, 11). Despite these advances, the mechanistic contribution of *EGR1* to prostate cancer metastasis is poorly defined.

Metastasis is the predominant cause of mortality in prostate cancer (12). Bone metastasis occur in 90% of metastatic PC patients and can lead to severe pain, pathological fracture, nerve compression and hypercalcemia (13). Prostate cancer brain metastasis is rare and often represents an end-stage lethal progression (14-17). We previously characterized a prostate cancer xenograft model that develops bone and brain metastasis dependent upon Ras pathway activation in the DU145/RasB1 cell line (18). Various genetically-engineered mouse models, additional human prostate cancer cell line models, and genetic and histological analyses of primary clinical tissues have contributed to the conclusion that Ras pathway activation is associated with prostate cancer metastasis (19-24).

In the DU145/RasB1 model, we previously identified FN14 (TNFRSF12A) as an overexpressed receptor that is necessary for efficient metastatic colonization (25). FN14 binds the TNF family ligand, TWEAK, one consequence of which is initiation of NF-κB

signaling. The downstream targets of the TWEAK-FN14 pathway that contribute to metastatic properties, however, have yet to be characterized in prostate cancer cells. In this study, we identify *EGR1* as a major downstream effector of the TWEAK-FN14 pathway and demonstrate that *EGR1* promotes prostate cancer bone and brain metastasis. We show that EGR1 regulates angiogenic and osteoclastogenic factors in PC, providing novel mechanistic insights into the role of EGR1 in prostate cancer metastasis.

Results

EGR1 expression is dysregulated in advanced PC

To investigate the downstream targets of the TWEAK-FN14 pathway, we analyzed the gene expression profile of highly metastatic DU145/RasB1 (B1) cells before and after treatment with TWEAK. Microarray analysis revealed a small number of differentially expressed genes, including the transcription factor, early growth response gene family (EGR1-4) (Fig 1A). *EGR1*, the most extensively studied of the family members, was the most highly expressed (Fig 1B). Validation PCR analysis demonstrated EGR1 as well as the NF-κB targets, IL-8 and IκBα, were stimulated by TWEAK-FN14 pathway activation (Fig 1B). To validate the microarray result at the protein level, DU145 B1 cells were treated with TWEAK for various times. Nuclear EGR1 protein levels transiently increased between 15 and 120 minutes after TWEAK addition (Fig 1C). Depletion of FN14 with shRNA blocked the EGR1 nuclear protein levels stimulated by TWEAK treatment (Fig 1C), demonstrating that EGR1 induction was a specific consequence of FN14 receptor engagement.

To determine whether EGR1 may play a role in clinical prostate cancer progression, we analyzed the gene expression of *EGR1* in samples of primary prostate cancer (8) with Gleason ≥7 as well as in a metastatic castration resistant prostate cancer (mCRPC) cohort composed of adenocarcinoma and enriched for neuroendocrine histologies (26). The results indicated that *EGR1* expression in primary prostate cancer was relatively uniform with only 6% demonstrating an mRNA expression z-score ≥2. By contrast, mCRPC patient samples represented a broad distribution with 40% having z-scores ≥2 (Fig 1D). Average *EGR1* expression between adenocarcinoma (mCRPC-Adeno) and neuroendocrine (mCRPC-NE) samples showed no significant difference, suggesting that *EGR1* levels were not associated with a specific pathological phenotype in these patient samples (Fig 1E). Collectively, these data indicate that *EGR1* is increased in response to TWEAK-FN14 pathway activation in DU145/RasB1 cells and that *EGR1* is elevated in a subset of clinical mCRPC samples.

The TWEAK-FN14 pathway induces EGR1 expression via MEK/ERK signaling

Previously, we demonstrate that the NF-κB p50/p65 pathway is a downstream mediator of TWEAK-FN14 in DU145 B1 cells (25). To determine whether EGR1 is downstream of the NF-κB pathway, we used DU145 B1/ IκBαSR cells, a cell line expressing a doxycycline-inducible, degradation-resistant IκBα super repressor (IκBαSR) that blocks both canonical and noncanonical NF-κB pathway by preventing the nuclear translocation of RELA (p65) and indirectly inhibiting synthesis of the NFKB2 (p52) precursor, p100 (27). Prior doxycycline induction of IκBαSR abolished TWEAK-stimulated nuclear translocation of p65 and p52, whereas EGR1 nuclear protein was still increased by TWEAK treatment (Fig

2A). This result suggested that NF-κB is not upstream of EGR1. To investigate whether EGR1 is required for activation of the NF-κB pathway, we used lentivirus-encoded shRNAs to knock down EGR1 in DU145/RasB1 cells. The data demonstrated that despite decreased EGR1 levels in the nucleus, both p65 and p52 nuclear protein translocation were still stimulated by TWEAK treatment in DU145 B1/ EGR1shRNA cells (Fig 2B), indicating that EGR1 is not upstream of NF-κB. Decreased levels of EGR1 did not appear to be compensated for by EGR2, EGR3, or EGR4 (Supplementary Fig 1). These data suggest that EGR1 and NF-κB are independent pathways stimulated by TWEAK engagement of FN14.

It has been reported that MEK/ERK signaling is stimulated downstream of FN14 ligation (28). Therefore, DU145 B1 cells were stimulated by TWEAK with or without the MEK1/2 inhibitor AZD8330, and nuclear EGR1 levels were determined. As shown in Figure 2C, prior treatment with AZD8330 blocked TWEAK-stimulated ERK1/2 phosphorylation and reduced EGR1 nuclear protein levels (Fig 2C), showing that EGR1 induction requires MEK/ERK signaling.

EGR1 is essential to the invasiveness of DU145/RasB1

To characterize the biological function of EGR1 in DU145 B1 cells, we first determined the effect of *EGR1* depletion on *in vitro* cell proliferation and *in vivo* tumorigenesis using either lentivirus empty vector control (DU145 B1/ EV) or one of two DU145 B1/ EGR1shRNA cell lines (shRNA11 and shRNA51) (Fig 2B). Our results revealed that decreased levels of EGR1 slightly reduced the growth rate of DU145 B1 cells but had no effect upon tumorigenesis (Fig 2D **and** E).

To assess the role of EGR1 in prostate cancer invasiveness, we performed invasion assays by seeding DU145 B1/ EV and DU145 B1/ EGR1shRNA cells on Matrigel-coated Transwell dishes. EGR1 depletion significantly reduced the number of invading DU145 B1 cells *in vitro* after 12 hours (Fig 2F), suggesting that EGR1 influences the invasiveness of prostate cancer cells. Adhesion and migration are two components that contribute to tumor invasiveness. However, as shown in Supplementary Figs 2A, B **and** C, decreased invasiveness cannot be accounted for by reduced adhesion to fibronectin, collagen I, collagen IV, or fibrin or by decreased migration ability.

EGR1 promotes experimental prostate cancer bone and brain metastasis

DU145 B1/ EV or DU145 B1/ EGR1shRNA cell lines (shRNA11 and shRNA51) (Fig 2B) were used to investigate the influence of EGR1 levels on metastatic capability. Following inoculation to the left cardiac ventricle, mice bearing either of the DU145 B1/ EGR1shRNA cells developed significantly less bone (Fig 3A **and** Fig 3B) and brain metastases (Fig 3A **and** Fig 3C) compared with mice bearing DU145 B1/ EV cells, as measured by total bioluminescent imaging (BLI) signal. The reduced luminescence in *EGR1* depleted lines was a consequence of reduced numbers of bone (Fig 3D) and brain metastatic foci (Fig 3E) as well as decreased tumor sizes. These results suggested that EGR1 contributes to the metastatic colonization of this aggressive prostate cancer model. In addition, mice inoculated with DU145 B1/ EGR1shRNA cells demonstrated less metastasis-associated

morbidity as they maintained their body weight while mice bearing DU145 B1/ EV cells did not (Fig 3F).

We previously demonstrated that NF-κB signaling is required for metastasis in the DU145 B1 xenograft model (25). This study indicated that EGR1 was necessary for PCa metastasis (Fig 3) and that the TWEAK-FN14 pathway induced EGR1 expression via MEK/ERK-dependent, NF-κB-independent fashion (Fig 2A, B **and** C), leading to the question of whether NF-κB signaling and EGR1 additively promote prostate cancer metastasis. To address this question in the DU145 B1model, we inhibited each pathway singly or together and measured bone and brain metastasis. However, since the tumor burden was so significantly reduced by blocking the NF-kB pathway alone, further blockade of EGR1 showed no additional reduction in tumor burden or the kinetics of metastasis development (Supplementary Fig 3A-D).

We also asked whether EGR1 expression contributes to bone metastasis in other models. Currently, there are relatively few bone metastasis models. Although prostate cancer-derived PC3 cells form bone metastasis, PC3 cells do not express detectable EGR1 protein (Supplementary Fig 4A). The MDA-MB-231 breast cancer cell line expressed EGR1 in a TWEAK-independent fashion at five to ten fold lower levels than DU145 B1 cells (Supplementary Fig 4A). We used lentivirus-encoded shRNAs to knock down EGR1 in MDA-MB-231 cells. The data demonstrated that EGR1 level was modestly reduced in two MDA-MB-231/ EGR1shRNA cell lines (shRNA51 and shRNA80) compared to cells transduced with lentivirus empty vector control (EV) (Supplementary Fig 4B). MDA-MB-231/ EV and two MDA-MB-231/ EGR1shRNA cell lines (shRNA51 and shRNA80) were inoculated into the left cardiac ventricle. Our results showed no significant difference of bone (Supplementary Fig 4C) or brain (Supplementary Fig 4D) tumor burden between mice bearing either of the MDA-MB-231/ EGR1shRNA cells and mice bearing MDA-MB-231/ EV cells, as measured by total bioluminescent imaging (BLI) signal. Taken together, these data suggest that the contribution of EGR1to bone metastasis is dependent upon cellular context (1, 33).

EGR1 stimulates angiogenesis in bone and brain metastases of DU145/RasB1

Our previous work characterized DU145 B1 cells as highly angiogenic (34). Since EGR1 has been increasingly recognized as a regulator of angiogenesis, we analyzed the blood vessel density, using the CD34 endothelial marker, within bone and brain metastatic lesions of DU145 B1/ EV and DU145 B1/ EGR1shRNA derived tumors. Interestingly, for both bone and brain metastases, depleting EGR1 significantly reduced the relative blood vessel area in tumors (Fig 4A, B, C **and** D). Because angiogenesis increases with tumor size and because *EGR1*-depleted metastases were on average smaller than DU145 B1/ EV metastases, we determined the blood vessel density relative to tumor area across a range of metastases collected at various time points. Our data did not support tumor size as an explanation for EGR1 correlated angiogenesis. As shown in Figs 4E, F, G **and** H, there was a trend that did not reach statistical significance in DU145 B1/ EV bone metastasis correlating vessel density and tumor size. However, there was no significant correlation

between blood vessel density and tumor size in DU145 B1/ EGR1shRNA bone and brain metastasis or DU145 B1/ EV brain metastasis.

EGR1 stimulates osteoclastogenesis in bone metastases

To further characterize the phenotype of bone metastasis, we analyzed x-ray images of mice bearing DU145 B1/ EV and DU145 B1/ EGR1shRNA tumors, which revealed mainly osteolytic metastases with an osteoblastic component (Fig 3A). To determine the role of EGR1 in the development of DU145 B1-mediated osteolysis, we quantified the osteolytic area on radiographic imaging of long bones in DU145 B1/ EV and DU145 B1/ EGR1shRNA bearing mice. The data demonstrated that depleting *EGR1* significantly decreased the osteolytic lesion area (Fig 5A **and** B). Consistent with this, histological analysis indicated that EGR1 knockdown significantly reduced the number of tartrate-resistant acid phosphatase-positive ($TRAP^+$) osteoclasts on bone-tumor interface (Fig 5A **and** C).

EGR1 regulates angiogenic and osteoclastogenic factors expression in prostate cancer

To begin addressing the relationship of the model described here to clinical prostate cancer, we asked whether *EGR1* levels are correlated with angiogenic and/or osteoclastogenic factor RNA levels in clinical prostate cancer data sets. For primary prostate cancer samples (8), we limited our analysis to Gleason score ≥7 samples, and the 25% of patient samples (n=113) with the highest *EGR1* expression were compared to the 25% of patient samples (n=113) with the lowest *EGR1* expression levels (Fig 6A). Gene set enrichment analysis (GSEA) revealed that the hallmark angiogenesis gene set was significantly enriched in the top quartile as compared to the bottom quartile of patient samples defined by *EGR1* expression (Fig 6B). Similarly, *EGR1* levels were correlated with the angiogenic signature in a phenotypically diverse data set of CRPC-adeno and CRPC-NE metastases (Fig 6C) (26). The distribution of gene expression making up the angiogenic signature are shown for CRPC samples in Supplementary Fig 5. A similar analysis was performed for osteoclastogenic genes. *EGR1* clearly clustered with global osteoclastogenic signature genes (Supplementary Fig 6) comparing the top and bottom *EGR1* expression quartiles for primary prostate cancer with Gleason scores ≥7. In addition, across all samples of Gleason score ≥7, *EGR1* positively correlated with 9 osteoclastogenic factors, including *LIF, IL1B, OSM, CSF3, CCL2, TNF, VCAM1, CSF1 and PTHLH* RNA levels (Supplementary Table 1).

EGR1 is induced by TWEAK in DU145 B1 cells. To determine whether TWEAK stimulated pro-angiogenic and/or osteoclastogenic factors via an EGR1-dependent mechanism, we treated DU145 B1/ EV and DU145 B1/ EGR1shRNA cells with TWEAK and performed qRT-PCR to detect gene expression of 47 pro-angiogenic/osteoclastogenic factors (Supplementary Table 2) (35, 36). TWEAK treatment increased gene expression for 12 pro-angiogenic factors in DU145 B1/ EV cells, including VEGFA, PDGFA, TGFB1, HIF1A, FGF2, SPP1, IL6, TGFA, ITGAV, EFNA1, IL8, and CXCL1 (Fig 6D). In addition, TWEAK treatment increased gene expression for the osteoclastogenic factors, CSF2 and TNFα (Fig 6D). Interestingly, some angiogenic factors such as CXCL1, IL6, TGFB1, and SPP1 have been found to also influence osteoclast and/or osteoblast development and function (37-40). Depletion of *EGR1* inhibited induction of these genes found to be regulated by TWEAK and

returned many but not all of the effected RNA levels to baseline (Fig 6D). IL8, a known NF-κB target, was only partially inhibited by EGR1 depletion, suggesting additive regulation by EGR1 and NF-κB. These data suggested that TWEAK stimulation of pro-angiogenic factors in the DU145 B1 model is mediated in large part by EGR1. We asked whether EGR1-regulated, soluble osteoclastogenic factors could be functionally detected in DU145 B1 cell culture supernatants. We performed an *in vitro* osteoclastogenesis assay that measured osteoclast maturation of a mouse monocyte cell line. RAW264.7 were primed with RANKL for 2 days, cultured with conditioned media (CM) from DU145 B1/ EV or either of DU145 B1/ EGR1shRNA cells for additional 2 days followed by TRAP staining (Supplementary Fig 7A). As shown in Supplementary Fig 7B **and** C, CM from DU145 B1/ EV induced significantly more $TRAP^+$ osteoclasts compared with CM from DU145 B1/ EGR1shRNA cells. These results demonstrate that EGR1 plays a role in the production of soluble osteoclastogenic factors.

Finally, we determined for those angiogenic/osteoclastogenic genes regulated in the DU145 B1 cells by EGR1 (26), whether evidence exists for similar regulation in clinical PC samples. As shown in Fig 6E, *EGR1* levels in clinical samples correlated with *IL6, IL8*, and *TNF* in primary prostate cancer samples and with *PDGFA, CSF2, ITGAV* and *CXCL1* in mCRPC samples (Fig 6F). Notably, *EGR1* did not correlate with *FN14* levels, however. This may be due to the fact that EGR1 is regulated by various upstream pathways (see Discussion). In addition, we have observed a lack of correlation between FN14 RNA and protein in some model systems, suggesting that *FN14* RNA cannot be used in correlation analyses.

Discussion

Using an experimental metastasis model and correlative analyses of clinical samples, we show that EGR1 contributes to prostate cancer metastasis, probably as a result of regulating a variety of angiogenic/osteoclastogenic/immune modulatory factors. EGR1 is necessary for efficient bone and brain metastasis in the AR-independent, DU145/RasB1 model of experimental prostate cancer metastasis. EGR1 has been hypothesized to play various roles in prostate cancer pathogenesis, including castration resistance, extracellular matrix degradation, apoptosis, and cancer progression (1, 41). The data presented here directly address a role for *EGR1* in prostate cancer metastasis. Importantly, for experimental metastasis, *EGR1* depletion had relatively little effect upon *in vitro* growth or tumorigenesis, but instead, decreased metastatic efficiency and reduced growth in those metastases that did arise (Figures 2 and 3). *EGR1* depleted metastases demonstrated less angiogenesis in the brain and bone and less osteoclast activity in the bone, characteristics that anticipate reduced growth (Figures 4 and 5). The analysis of large primary and metastatic clinical sample data sets was consistent with highly deregulated *EGR1* expression in a large proportion of metastatic samples (Figure 6).

The role of EGR1 as a transcriptional regulator of angiogenic factors has been increasingly recognized. For example, EGR1 has recently been shown to be a key target of the miR-192 regulatory network that is predictive of poor clinical outcome in several cancer types as a result of modulating the angiogenic switch (36). Interestingly, there are several EGR1-

regulated genes encoding secreted factors, including TGFβ, IL-8, IL-6, SPP1, and CXCL-1, that influence osteoclast differentiation in addition to angiogenesis (37-40). Consistent with this, EGR1 expression influenced the extent of soluble osteoclastogenic activity produced in cell supernatants of DU145 B1 cells (Supplemental Fig 7). In agreement with the experimental data presented here, EGR1 expressing clinical prostate cancer samples were enriched for expression of global angiogenic and osteoclastogenic signatures (Figs. 6B&C, Supplemental Figs. 2 & 3). In addition, experimentally-validated individual EGR1-regulated angiogenic (*PDGFA)* and osteoclastogenic (*CSF2, TNF)* genes as well as those effecting both of these processes (*IL6, IL8,* and *CXCL1*) demonstrated a significant correlation with *EGR1* levels in clinical data sets. Our observations in DU145 B1 cells are corroborated by reports using other tissue types that demonstrate EGR1 binding to the *FGF2* (42)*, PDGFA* (43), *TNF* (44), *IL8* (45) and *TGFB1* (46) promoters. Although EGR1/2 have been shown to be involved in osteogenic differentiation (47), an involvement in the development of bone metastasis has not been widely appreciated. There is a known requirement for osteoclastogenesis, even in the formation of osteoblastic metastasis (48).

We show here, consistent with other reports, that EGR1 induction was dependent upon MEK-ERK pathway signaling (1). The RAS/RAF/ERK pathway is dysregulated in 43% of primary PC and >90% of PC metastasis when considering combined copy number alterations, transcriptomic and mutational data (24). Similarly, RAF and ERK activation, as determined by tissue staining, occur at high frequency and have been observed to increase with PC progression (20, 49). We show here that TWEAK binding to the FN14 receptor in DU145/Ras cells initiates MEK-dependent, NF-kB-independent *EGR1* expression. *EGR1* is an early response gene regulated by a variety of soluble factors and stress stimuli. For example, *EGR1* is induced in DU145 cells by diverse stimuli, including CXCL5, hypoxia, and radiation (50-52). Thus, it is likely that elevated *EGR1* expression in metastatic PC clinical samples may be secondary to a variety of mutational or microenvironmental effects, including but not limited to FN14 engagement. Taken together, our data identify a MEK/ERK-EGR1 pathway, an important physiological consequence of which is increased angiogenesis and osteoclastogenesis contributing to PC metastasis. These data provide a rationale for development of EGR1-targeted therapies and suggest consideration of MEK-dependent EGR1 inhibition as one component of a therapeutic approach to treating advanced metastatic PC.

Materials and Methods

shRNA-mediated gene silencing in DU145/RasB1 and MDA-MB-231 cells

DU145, MDA-MB-231 and PC3 cells were obtained from ATCC. All genetically engineered cell lines were established using lentiviral vectors following standard procedures (18). DU145/RasB1 cells infected with a pFUGW lentiviral expression clone containing mutant IkBα super repressor (IkBαSR; IkBaS32A, S36A) under the control of the TRE3G promoter with an IRES-mCherry reporter have been described (25). IkBαSR expression was induced with 1 mg/mL doxycycline. EGR1 gene was silenced with *EGR1* shRNAs in the pGIPZ lentiviral vector, designed by The RNAi Consortium (TRC, Open Biosystems) and targeting the following sequences: 5’-TATCCCATGGGCAATAAAG −3’ (shRNA11), 5’-

ACATTCTGGAGAACCGAAG −3’ (shRNA28), 5’-ATACACCACATATCCCATG-3’ (shRNA51), 5’-TTGTCTGCTTTCTTGTCCT −3’ (shRNA80), 5’-TAGGGTAGTTGTCCATGGT −3’ (shRNA83).

Animal experiments

6- to 8-week-old male athymic nude mice (Ncr *nu/nu*) and NOD *scid* gamma were obtained from the National Cancer Institute, Frederick, MD. Animal care was provided in accordance with the procedures outlined in the *Guide for the Care and Use of Laboratory Animals.* Prior to injection, cells were harvested from subconfluent cell culture with trypsin, resuspended in RPMI 1640 with10% fetal bovine serum, rotated at room temperature for 1 hour, spun down, and washed in PBS. Cells were counted and diluted to the appropriate concentration.

Systemic tumor metastasis

A total of 10^5 tumor cells in 0.1 ml of PBS were inoculated into the left cardiac ventricles of male nude mice or NOD *scid* gamma after anesthetizing them with 1.5% isoflurane. Each experimental group included a minimum of 5 mice. Mice were allocated to each group randomly. Mice were euthanized after weight loss of >10% body weight or after demonstrating signs of paralysis. Four long bones (two front limbs with scapulae and two hind limbs), spines and brain were collected and fixed in 10% paraformaldehyde for histological analysis (Histoserv, Inc., Germantown, MD, USA).

Bioluminescent imaging and analysis

Mice were anesthetized with 1.5% isoflurane. D-Luciferin (Gold Biotechnology Inc., St. Louis, MO, USA) was injected at 150 mg/kg (body weight). Five minutes later, bioluminescent images were acquired with an IVIS imaging system (PerkinElmer, Waltham, MA, USA). Analysis was performed by using LivingImage software (PerkinElmer) by measuring the photon flux within a region of interest drawn around the bioluminescence signals. Blank regions of interest were also measured for each scan and deducted from each tumor photon flux to normalize. Ventral scans were used for quantification of all jaw and leg tumors. Dorsal scans were used for brain tumor quantifications. The imaging and analysis were performed blindly.

Tumorigenesis assays

A total of 5×10^6 DU145/RasB1 cells in 50 μl PBS was mixed 1:1 with growth factor-reduced Matrigel (Corning Inc., Corning, NY, USA) immediately prior to injection. Cells were injected bilaterally subcutaneously into the shoulders and flanks of nude mice. The tumor size was measured with calipers. The tumor volume was calculated from the following formula: tumor volume = $4/3\ \pi XL/2\ (W/2)^2$.

Genetic analysis of prostate cancer patient samples

To investigate whether EGR1 clusters with global gene expression of pro-angiogenic factors or osteoclastogenic factors in prostate cancer. We obtained data for the TCGA primary prostate cancer (8) and the NEPC WCM 2016 mCRPC (26) cohorts and generated heatmaps

using the HeatMapImage tool (https://software.broadinstitute.org/cancer/software/genepattern/).

To analyze the correlation of EGR1 and pro-angiogenic or osteoclastogenic genes in prostate cancer, we retrieved data for primary prostate cancer (8) and mCRPC (26) cohorts from cBioPortal. The mRNA data were log2-transformed by Excel 2016. The correlation between EGR1 and pro-angiogenic or osteoclastogenic genes was then analyzed by Pearson correlation test and plotted using GraphPad Prism 7.

GSEA analysis

For the gene set enrichment analysis (GSEA), GSEA software was downloaded from the Broad Institute. The 25% of samples (n=113) with the highest EGR1 expression and the 25% of samples (n=113) with the lowest EGR1 expression from the TCGA primary prostate cancer cohort (8) were assigned to two groups. Patient samples with the highest (n=10) or lowest (n=10) EGR1 expression in the NEPC WCM 2016 mCRPC cohort (26) were assigned to two groups. The number of permutations was set to 1 000, and the permutation type was set to 'phenotype'. A normalized enrichment score (NES) and false discovery rate (FDR) were calculated by the program.

Microarray

DU145/RasB1 cells were treated with TWEAK (25ng/mL, R&D Systems, Minneapolis, MN, USA) for 60 min. Total RNA was extracted using mirVana Isolation Kit (Thermo Fisher Scientific, Waltham, MA, USA). After TWEAK treatment, samples were validated for increased expression levels of known NFκB target genes, IL8 and IκBα, and submitted for microarray analysis. Microarray analysis was performed with Affymetrix Human Genome U133A 2.0 Array. Fold changes in gene expression were determined by ANOVA using Partek Genomics Suite (Partek, Chesterfield, MO, USA).

Real-Time PCR

Quantative PCR was performed using SYBR Green Mastermix (Roche, Basel, Switzerland) and the Stepone Plus RT PCR System (Applied Biosystems, Foster City, CA, USA). All reactions were run in triplicate using primers listed in Supplementary Table 3. Values were normalized to GAPDH unless otherwise stated. Each experiment was repeated three times.

Western blotting

Nuclear and cytoplasmic protein fractions were separated by using NE-PER™ Nuclear and Cytoplasmic Extraction Kit (Thermo Fisher Scientific, Waltham, MA, USA). Western blot was performed by using precast 4-20% Precast Gels (Bio-Rad, Hercules, CA). Antibodies used for analysis were EGR1 (1:1 000 dilution, Cell Signaling Technology, Danvers, MA, USA), p65 (1:1 000, Santa Cruz Biotechnology, Inc. Dallas, Texas, USA), p52 (1:1 000, Millipore), LaminB1 (1:1 000 dilution, Abcam, Cambridge, MA, USA), IκBα (1:1 000, Santa Cruz,), FN14 (1:1 000, Abcam) and α-tubulin (1:2 000 dilution, MilliporeSigma, Burlington, MA, USA), followed by detection using appropriate anti-mouse or anti-rabbit secondary antibodies (GE Healthcare Life Sciences, Pittsburgh, USA 1:2 000). EGR1, p65, p52 and LaminB1 protein were detected in the nuclear extracts, and FN14, IκBα and α-

tubulin protein were detected in the cytoplasmic extracts. All western blots were representative of a minimum of three experiments.

Invasion assay

Invasion chambers were prepared by coating 8 μM pore, 24-well format membranes (BD Biosciences, San Jose, CA, USA) with 100 μL (0.5 mg/mL) Matrigel (Corning Inc.) per well and incubating them overnight at room temperature. Cells were harvested with trypsin, allowed to recover for 1 hour with rocking in 10% FCS, washed in PBS, and resuspended to 10^6 cells/mL. 200 μL of cells was placed into the upper chamber while 500 μL RPMI 1640 was placed into the bottom. Cells were incubated for 12 hours at 37°C/5% CO2. Invasion was assayed as previously described (53). Each experiment was repeated three times.

Histology, immunohistochemistry (IHC) and histomorphometric analysis

Long bones were decalcified in 10% EDTA, embedded in paraffin and sections were stained with hematoxylin, eosin (H&E) and orange G. All mouse brains were stained with H&E. For IHC, slides were autoclaved at 121°C for 10 min in target retrieval solution (DAKO, Santa Clara, CA, USA), followed by CD34 antibody (1:2 000, Abcam). Tartrate-resistant acid phosphatase (TRAP) staining was performed as previously described (18). For histomorphometric analysis, bright-field microscopic images were acquired randomly with a AxioScan Z1 microscope using a 20X/NA 0.8 plan apochromat objective (Zeiss, Oberkochen, Germany). CD34-stained blood vessel areas were quantified using ImageJ (NIH, Bethesda, MD, USA) as described previously (34). $TRAP^+$ osteoclast number per millimeter of tumor/bone interface was counted at 20X magnification as described previously (34, 54). All the analysis was performed blindly.

In vitro growth determinations

Cells were seeded in six replicates in 96-well plates at densities of 2×10^3 cells per well. Each day, one plate was stained with crystal violet fixative solution for 30 min, rinsed in distilled water, and allowed to air dry. At the end of the experiment, crystal violet was dissolved by adding 100μl of 50% ethanol containing 0.1 M sodium citrate to each well, and the absorbance was quantified at a 540nm wavelength on a plate reader. Each experiment was repeated three times.

Radiography

Animals were x-rayed against the detector, and exposed with an x-ray at 35 KVP for 5 s by using a Faxitron Digital Radiographic Inspection unit (Faxitron, Tucson, AZ, USA) as previously described (54). Osteolytic lesions were identified on radiographs as demarcated radiolucent lesions in the bone and quantified blindly by using ImageJ (NIH).

Wound healing Assays

DU145 B1/ EV and DU145 B1/ EGR1shRNA11 cells were seeded at a density of 5×10^6 cells in the 10 cm dish to attain hyperconfluency after 24 hours. The media was changed the following day and the hyperconfluent 10 cm dish was scratched with a silicon-coated 1 mL pipette tip. A timed series of phase contrast pictures were taken at day 0, 1 and 2 using a

AxioObserver Z1 Fluorescent Microscope (Zeiss). Plates were marked so that pictures were taken at precisely consistent positions along each individual scratch. Wound healing assays were quantified as described previously (55). Each experiment was repeated three times.

Osteoclastogenesis Assay

RAW264.7 cells were provided by Dr. Yibin Kang from Princeton University. RAW264.7 cells were seeded in triplicate at a density of $1.25 \times 10^4/cm^2$ in a 12-well dish. After 24 hours, cell cultures were supplemented with RANKL (20ng/ml, R&D Systems, Minneapolis, MN, USA) for 2 days (priming) followed by application of 10% conditioned media from DU145 B1/ EV or either of DU145 B1/ EGR1shRNA cells for additional 2 days. Cells were fixed with 4% paraformaldehyde and TRAP stained as previously described (18). Images were recorded randomly using a AxioObserver Z1 Fluorescent Microscope (Zeiss, Oberkochen, Germany) and quantified blindly. Osteoclasts were identified as TRAP-positive cells with three or more nuclei. Each experiment was repeated twice.

Statistical methods

GraphPad Prism 7 was used for graphs and statistics. Data were expressed as mean ± SEM or box-and-whisker plots. All data were analyzed using the two-tailed Student *t* test for comparison of two groups or one-way ANOVA for three groups or more. The Pearson test was used to assess the correlation study. Log-rank test (Wilcox survival) was used to analyze survival data. Differences were considered statistically significant when the *P*-value was <0.05.

Supplementary Material

Refer to Web version on PubMed Central for supplementary material.

References

1. Gitenay D, Baron VT. Is EGR1 a potential target for prostate cancer therapy? Future oncology. 2009;5(7):993–1003. [PubMed: 19792968]
2. Krones-Herzig A, Mittal S, Yule K, Liang H, English C, Urcis R, et al. Early growth response 1 acts as a tumor suppressor in vivo and in vitro via regulation of p53. Cancer Res. 2005;65(12):5133–43. [PubMed: 15958557]
3. Yamamoto C, Basaki Y, Kawahara A, Nakashima K, Kage M, Izumi H, et al. Loss of PTEN expression by blocking nuclear translocation of EGR1 in gefitinib-resistant lung cancer cells harboring epidermal growth factor receptor-activating mutations. Cancer Res. 2010;70(21):8715–25. [PubMed: 20959484]
4. Zagurovskaya M, Shareef MM, Das A, Reeves A, Gupta S, Sudol M, et al. EGR-1 forms a complex with YAP-1 and upregulates Bax expression in irradiated prostate carcinoma cells. Oncogene. 2009;28(8):1121–31. [PubMed: 19137013]
5. Abdulkadir SA, Qu Z, Garabedian E, Song SK, Peters TJ, Svaren J, et al. Impaired prostate tumorigenesis in Egr1-deficient mice. Nat Med. 2001;7(1):101–7. [PubMed: 11135623]
6. Eid MA, Kumar MV, Iczkowski KA, Bostwick DG, Tindall DJ. Expression of early growth response genes in human prostate cancer. Cancer research. 1998;58(11):2461–8. [PubMed: 9622090]
7. Mulholland DJ, Tran LM, Li Y, Cai H, Morim A, Wang S, et al. Cell autonomous role of PTEN in regulating castration-resistant prostate cancer growth. Cancer Cell. 2011;19(6):792–804. [PubMed: 21620777]

8. Cancer Genome Atlas Research N. The Molecular Taxonomy of Primary Prostate Cancer. Cell. 2015;163(4):1011–25. [PubMed: 26544944]
9. Yang SZ, Eltoum IA, Abdulkadir SA. Enhanced EGR1 activity promotes the growth of prostate cancer cells in an androgen-depleted environment. J Cell Biochem. 2006;97(6):1292–9. [PubMed: 16552752]
10. Yang SZ, Abdulkadir SA. Early growth response gene 1 modulates androgen receptor signaling in prostate carcinoma cells. J Biol Chem. 2003;278(41):39906–11. [PubMed: 12890669]
11. Adamson ED, Mercola D. Egr1 transcription factor: multiple roles in prostate tumor cell growth and survival. Tumour Biol. 2002;23(2):93–102. [PubMed: 12065847]
12. Wu JN, Fish KM, Evans CP, Devere White RW, Dall'Era MA. No improvement noted in overall or cause-specific survival for men presenting with metastatic prostate cancer over a 20-year period. Cancer. 2014;120(6):818–23. [PubMed: 24258693]
13. Mundy GR. Metastasis to bone: causes, consequences and therapeutic opportunities. Nat Rev Cancer. 2002;2(8):584–93. [PubMed: 12154351]
14. Tannock IF, de Wit R, Berry WR, Horti J, Pluzanska A, Chi KN, et al. Docetaxel plus prednisone or mitoxantrone plus prednisone for advanced prostate cancer. N Engl J Med. 2004;351(15):1502–12. [PubMed: 15470213]
15. Jemal A, Siegel R, Xu J, Ward E. Cancer statistics, 2010. CA Cancer J Clin. 2010;60(5):277–300. [PubMed: 20610543]
16. Caffo O, Gernone A, Ortega C, Sava T, Carteni G, Facchini G, et al. Central nervous system metastases from castration-resistant prostate cancer in the docetaxel era. J Neurooncol. 2012;107(1):191–6. [PubMed: 21989810]
17. Hatzoglou V, Patel GV, Morris MJ, Curtis K, Zhang Z, Shi W, et al. Brain metastases from prostate cancer: an 11-year analysis in the MRI era with emphasis on imaging characteristics, incidence, and prognosis. J Neuroimaging. 2014;24(2):161–6. [PubMed: 23279641]
18. Yin J, Pollock C, Tracy K, Chock M, Martin P, Oberst M, et al. Activation of the RalGEF/Ral pathway promotes prostate cancer metastasis to bone. Mol Cell Biol. 2007;27(21):7538–50. [PubMed: 17709381]
19. Aytes A, Mitrofanova A, Kinkade CW, Lefebvre C, Lei M, Phelan V, et al. ETV4 promotes metastasis in response to activation of PI3-kinase and Ras signaling in a mouse model of advanced prostate cancer. Proc Natl Acad Sci U S A. 2013;110(37):E3506–15. [PubMed: 23918374]
20. Kinkade CW, Castillo-Martin M, Puzio-Kuter A, Yan J, Foster TH, Gao H, et al. Targeting AKT/mTOR and ERK MAPK signaling inhibits hormone-refractory prostate cancer in a preclinical mouse model. J Clin Invest. 2008;118(9):3051–64. [PubMed: 18725989]
21. Min J, Zaslavsky A, Fedele G, McLaughlin SK, Reczek EE, De Raedt T, et al. An oncogene-tumor suppressor cascade drives metastatic prostate cancer by coordinately activating Ras and nuclear factor-kappaB. Nat Med. 2010;16(3):286–94. [PubMed: 20154697]
22. Mulholland DJ, Kobayashi N, Ruscetti M, Zhi A, Tran LM, Huang J, et al. Pten loss and RAS/MAPK activation cooperate to promote EMT and metastasis initiated from prostate cancer stem/progenitor cells. Cancer Res. 2012;72(7):1878–89. [PubMed: 22350410]
23. Ruscetti M, Quach B, Dadashian EL, Mulholland DJ, Wu H. Tracking and Functional Characterization of Epithelial-Mesenchymal Transition and Mesenchymal Tumor Cells during Prostate Cancer Metastasis. Cancer Res. 2015;75(13):2749–59. [PubMed: 25948589]
24. Taylor BS, Schultz N, Hieronymus H, Gopalan A, Xiao Y, Carver BS, et al. Integrative genomic profiling of human prostate cancer. Cancer Cell. 2010;18(1):11–22. [PubMed: 20579941]
25. Yin J, Liu YN, Tillman H, Barrett B, Hewitt S, Ylaya K, et al. AR-regulated TWEAK-FN14 pathway promotes prostate cancer bone metastasis. Cancer research. 2014;74(16):4306–17. [PubMed: 24970477]
26. Beltran H, Prandi D, Mosquera JM, Benelli M, Puca L, Cyrta J, et al. Divergent clonal evolution of castration-resistant neuroendocrine prostate cancer. Nat Med. 2016;22(3):298–305. [PubMed: 26855148]
27. Cancro MP. Signalling crosstalk in B cells: managing worth and need. Nat Rev Immunol. 2009;9(9):657–61. [PubMed: 19704418]

28. Winkles JA. The TWEAK-Fn14 cytokine-receptor axis: discovery, biology and therapeutic targeting. Nat Rev Drug Discov. 2008;7(5):411–25. [PubMed: 18404150]
29. Liao Y, Shikapwashya ON, Shteyer E, Dieckgraefe BK, Hruz PW, Rudnick DA. Delayed hepatocellular mitotic progression and impaired liver regeneration in early growth response-1-deficient mice. The Journal of biological chemistry. 2004;279(41):43107–16. [PubMed: 15265859]
30. Mayer SI, Rossler OG, Endo T, Charnay P, Thiel G. Epidermal-growth-factor-induced proliferation of astrocytes requires Egr transcription factors. Journal of cell science. 2009;122(Pt 18):3340–50. [PubMed: 19706684]
31. Muller I, Rossler OG, Wittig C, Menger MD, Thiel G. Critical role of Egr transcription factors in regulating insulin biosynthesis, blood glucose homeostasis, and islet size. Endocrinology. 2012;153(7):3040–53. [PubMed: 22597533]
32. O'Donovan KJ, Tourtellotte WG, Millbrandt J, Baraban JM. The EGR family of transcription-regulatory factors: progress at the interface of molecular and systems neuroscience. Trends in neurosciences. 1999;22(4):167–73. [PubMed: 10203854]
33. Baron V, Adamson ED, Calogero A, Ragona G, Mercola D. The transcription factor Egr1 is a direct regulator of multiple tumor suppressors including TGFbeta1, PTEN, p53, and fibronectin. Cancer gene therapy. 2006;13(2):115–24. [PubMed: 16138117]
34. Yin JJ, Zhang L, Munasinghe J, Linnoila RI, Kelly K. Cediranib/AZD2171 inhibits bone and brain metastasis in a preclinical model of advanced prostate cancer. Cancer Res. 2010;70(21):8662–73. [PubMed: 20959486]
35. Starmans MH, Chu KC, Haider S, Nguyen F, Seigneuric R, Magagnin MG, et al. The prognostic value of temporal in vitro and in vivo derived hypoxia gene-expression signatures in breast cancer. Radiother Oncol. 2012;102(3):436–43. [PubMed: 22356756]
36. Wu SY, Rupaimoole R, Shen F, Pradeep S, Pecot CV, Ivan C, et al. A miR-192-EGR1-HOXB9 regulatory network controls the angiogenic switch in cancer. Nat Commun. 2016;7:11169. [PubMed: 27041221]
37. Chang J, Allen TD, Dexter TM. Long-term bone marrow cultures: their use in autologous marrow transplantation. Cancer Cells. 1989;1(1):17–24. [PubMed: 2701357]
38. Hardaway AL, Herroon MK, Rajagurubandara E, Podgorski I. Marrow adipocyte-derived CXCL1 and CXCL2 contribute to osteolysis in metastatic prostate cancer. Clin Exp Metastasis. 2015;32(4):353–68. [PubMed: 25802102]
39. Juarez P, Guise TA. TGF-beta in cancer and bone: implications for treatment of bone metastases. Bone. 2011;48(1):23–9. [PubMed: 20699127]
40. Manolagas SC. Birth and death of bone cells: basic regulatory mechanisms and implications for the pathogenesis and treatment of osteoporosis. Endocr Rev. 2000;21(2):115–37. [PubMed: 10782361]
41. Adamson E, de Belle I, Mittal S, Wang Y, Hayakawa J, Korkmaz K, et al. Egr1 signaling in prostate cancer. Cancer Biol Ther. 2003;2(6):617–22. [PubMed: 14688464]
42. Kundumani-Sridharan V, Niu J, Wang D, Van Quyen D, Zhang Q, Singh NK, et al. 15(S)-hydroxyeicosatetraenoic acid-induced angiogenesis requires Src-mediated Egr-1-dependent rapid induction of FGF-2 expression. Blood. 2010;115(10):2105–16. [PubMed: 20053757]
43. Silverman ES, Khachigian LM, Lindner V, Williams AJ, Collins T. Inducible PDGF A-chain transcription in smooth muscle cells is mediated by Egr-1 displacement of Sp1 and Sp3. Am J Physiol. 1997;273(3 Pt 2):H1415–26. [PubMed: 9321833]
44. Yao J, Mackman N, Edgington TS, Fan ST. Lipopolysaccharide induction of the tumor necrosis factor-alpha promoter in human monocytic cells. Regulation by Egr-1, c-Jun, and NF-kappaB transcription factors. J Biol Chem. 1997;272(28):17795–801. [PubMed: 9211933]
45. Singha B, Gatla HR, Manna S, Chang TP, Sanacora S, Poltoratsky V, et al. Proteasome inhibition increases recruitment of IkappaB kinase beta (IKKbeta), S536P-p65, and transcription factor EGR1 to interleukin-8 (IL-8) promoter, resulting in increased IL-8 production in ovarian cancer cells. J Biol Chem. 2014;289(5):2687–700. [PubMed: 24337575]

46. Liu C, Adamson E, Mercola D. Transcription factor EGR-1 suppresses the growth and transformation of human HT-1080 fibrosarcoma cells by induction of transforming growth factor beta 1. Proc Natl Acad Sci U S A. 1996;93(21):11831–6. [PubMed: 8876223]
47. Rostovskaya M, Donsante S, Sacchetti B, Alexopoulou D, Klemroth S, Dahl A, et al. Clonal Analysis Delineates Transcriptional Programs of Osteogenic and Adipogenic Lineages of Adult Mouse Skeletal Progenitors. Stem Cell Reports. 2018;11(1):212–27. [PubMed: 29937146]
48. Zhang J, Dai J, Qi Y, Lin DL, Smith P, Strayhorn C, et al. Osteoprotegerin inhibits prostate cancer-induced osteoclastogenesis and prevents prostate tumor growth in the bone. J Clin Invest. 2001;107(10):1235–44. [PubMed: 11375413]
49. Faltermeier CM, Drake JM, Clark PM, Smith BA, Zong Y, Volpe C, et al. Functional screen identifies kinases driving prostate cancer visceral and bone metastasis. Proc Natl Acad Sci U S A. 2016;113(2):E172–81. [PubMed: 26621741]
50. Sperandio S, Fortin J, Sasik R, Robitaille L, Corbeil J, de Belle I. The transcription factor Egr1 regulates the HIF-1alpha gene during hypoxia. Mol Carcinog. 2009;48(1):38–44. [PubMed: 18506761]
51. Tsai MH, Cook JA, Chandramouli GV, DeGraff W, Yan H, Zhao S, et al. Gene expression profiling of breast, prostate, and glioma cells following single versus fractionated doses of radiation. Cancer Res. 2007;67(8):3845–52. [PubMed: 17440099]
52. Kuo PL, Chen YH, Chen TC, Shen KH, Hsu YL. CXCL5/ENA78 increased cell migration and epithelial-to-mesenchymal transition of hormone-independent prostate cancer by early growth response-1/snail signaling pathway. J Cell Physiol. 2011;226(5):1224–31. [PubMed: 20945384]
53. Wang T, Ward Y, Tian L, Lake R, Guedez L, Stetler-Stevenson WG, et al. CD97, an adhesion receptor on inflammatory cells, stimulates angiogenesis through binding integrin counterreceptors on endothelial cells. Blood. 2005;105(7):2836–44. [PubMed: 15576472]
54. Yin JJ, Selander K, Chirgwin JM, Dallas M, Grubbs BG, Wieser R, et al. TGF-beta signaling blockade inhibits PTHrP secretion by breast cancer cells and bone metastases development. The Journal of clinical investigation. 1999;103(2):197–206. [PubMed: 9916131]
55. Jansson KH, Lynch JE, Lepori-Bui N, Czymmek KJ, Duncan RL, Sikes RA. Overexpression of the VSSC-associated CAM, beta-2, enhances LNCaP cell metastasis associated behavior. Prostate. 2012;72(10):1080–92. [PubMed: 22127840]

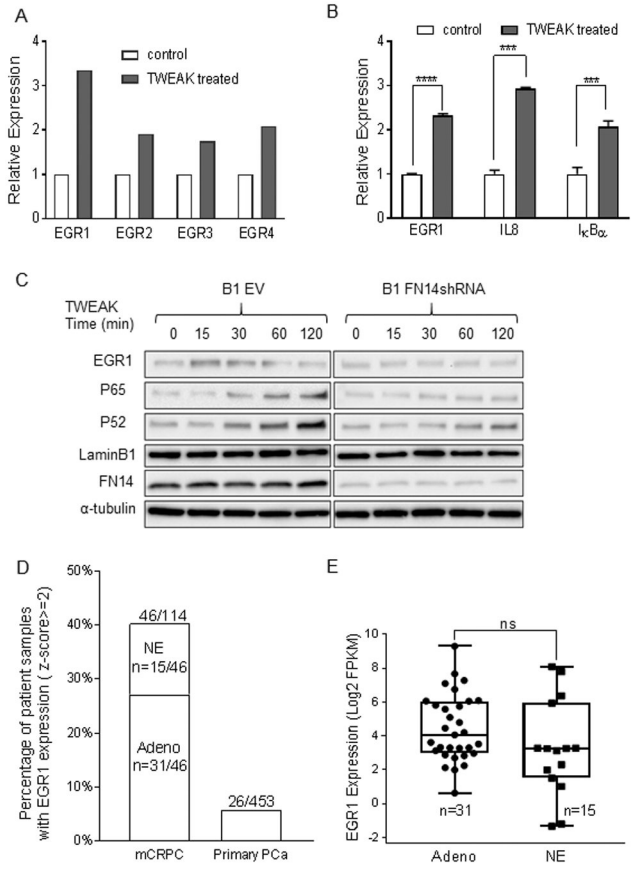

Figure 1. TWEAK-FN14 pathway activation stimulates *EGR1*, and dysregulated *EGR1* expression is observed in prostate cancer metastasis.

(**A**) Microarray analysis of *EGR1-4* in response to TWEAK (25ng/ml) treatment for 60 min. (**B**) qPCR analysis of *EGR1, IL8* and *NFKBIA* (IκBα*)* in DU145/RasB1 prostate cancer cell line treated with TWEAK (25ng/ml) for 1 hr. ***, P<0.001, ****, P < 0.0001.

(**C**) Western blot analysis of FN14, EGR1, NFKB2 (p52) and RELA (p65) in DU145/RasB1/EV and DU145/RasB1/FN14 shRNAs. Cells were treated with TWEAK for various times. FN14 was detected in the cytoplasmic fraction. p65, p52 and EGR1 were detected in the nuclear fraction. α-tubulin was the loading control for cytoplasmic extracts. LaminB1 was the loading control for nuclear extracts.

(**D**) Percentage of mCRPC and primary prostate cancer patient samples with *EGR1* expression z-score ≥2. The numbers on top of each bar indicate the ratio of patient samples with *EGR1* expression (z-score ≥2) over total samples in mCRPC or primary prostate cancer cohorts. The numbers inside the bar indicated the ratio of patient samples with *EGR1* expression (z-score ≥2) over total mCRPC-NE or mCRPC-Adeno samples.

(**E**) *EGR1* mRNA expression in NEPC WCM 2016 mCRPC-Adeno (n=31) or mCRPC-NE (n=15) patient samples with *EGR1* expression z-score≥2.0 in mCRPC cohort.

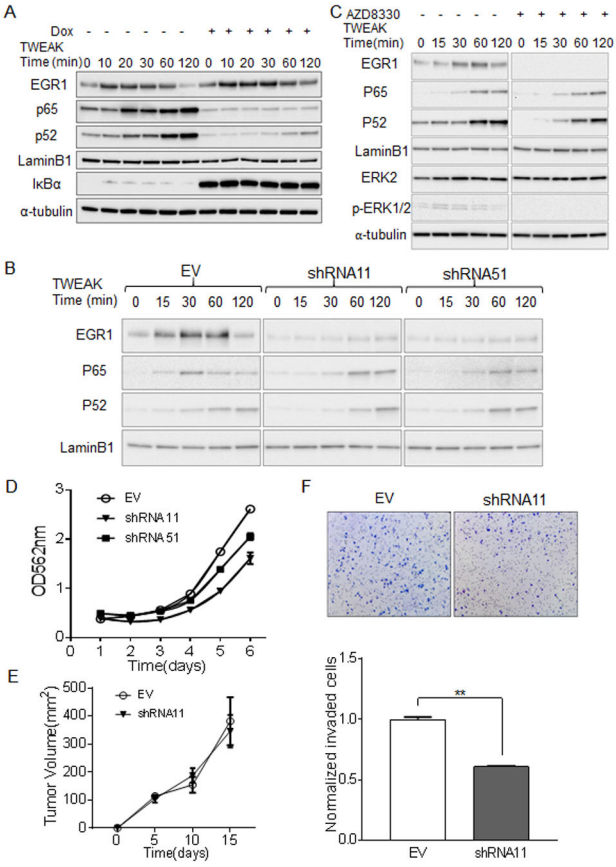

Figure 2. EGR1 is increased by TWEAK-FN14 activation through MEK/ERK signaling and contributes to invasiveness but not tumorigenesis.

(**A**) Western blot analysis of IκBα, p65, p52 and EGR1 in DU145/RasB1/ TRE3G-IκBαSR cells. Cells were treated with TWEAK (25ng/ml) for various times. IκBα was detected in the cytoplasmic fraction; p65, p52 and EGR1 were detected in the nuclear fraction.

(**B**) Western blot analysis of nuclear EGR1, p52 and p65 in DU145/RasB1/EV, DU145/RasB1/EGR1 shRNA11 and DU145/RasB1/EGR1 shRNA51. Cells were treated with TWEAK (25ng/ml) for various times.

(**C**) Western blot analysis of EGR1, p65, p52, ERK2 and p-ERK1/2 in DU145/RasB1. Cells were incubated with MEK1/2 inhibitor AZD8330 (1μM) for 2 hours before TWEAK treatment. ERK2 and p-ERK1/2 were detected in the cytoplasmic fraction. p65, p52 and EGR1 were detected in the nuclear fraction.

(**D**) Proliferation rate of DU145 B1/ EV, DU145 B1/ EGR1shRNA11 and DU145 B1/ EGR1shRNA51 in culture.

(**E**) Volumes of DU145 B1/ EV or DU145 B1/ EGR1shRNA11 tumors over time.

(**F**) Top panel: representative images of HEMA3-stained DU145 B1/ EV and DU145 B1/ EGR1shRNA11 cells following invasion for 12 hours. Bottom panel: quantification of invaded cells in transwell assay. **, P<0.01.

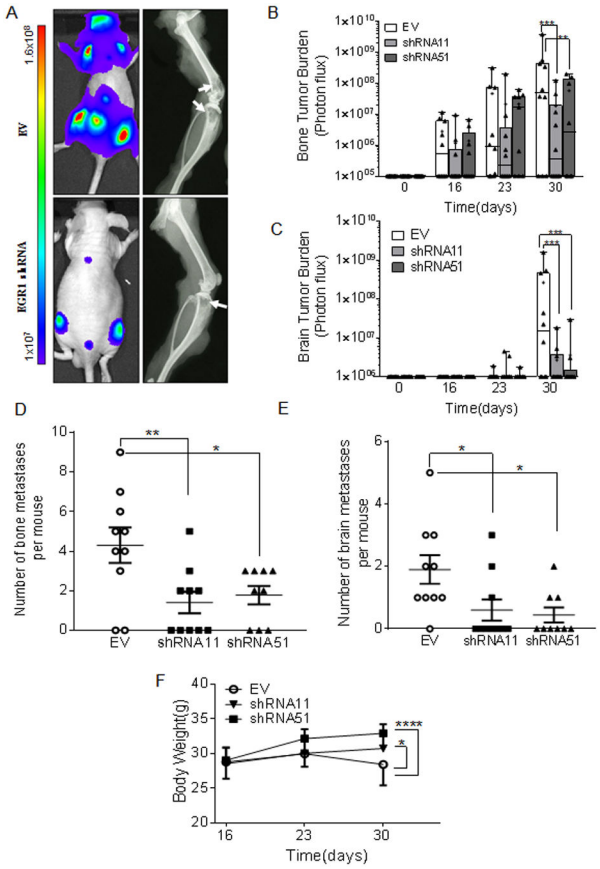

Figure 3. Blocking EGR1 expression inhibits prostate cancer metastases to bone and brain.

(**A**) Representative bioluminescent and x-ray images from mice bearing DU145 B1/ EV or DU145 B1/ EGR1shRNA metastasis. Arrows indicate osteolytic lesions.

(**B**) Quantification of bone metastasis burden shown as mean photonflux. EV and shRNA11: n=10 mice; shRNA51: n=9 mice; **, P<0.01; ***, P<0.001; the median value is indicated by a horizontal line within the box.

(**C**) Quantification of brain metastasis burden shown as mean photonflux. EV and shRNA11: n=10 mice per group; shRNA51: n=9 mice; ***, P<0.001; the median value is indicated by a horizontal line within the box.

(**D**) Number of bone metastatic foci per mouse from each experimental group determined using bioluminescent imaging.

(**E**) Number of brain metastatic foci per mouse from each experimental group determined using bioluminescent imaging.

(**F**) Average body weight of mice bearing DU145 B1/ EV or DU145 B1/ EGR1shRNA tumors over time following inoculation (EV, n= 10; shRNA11, n=10; shRNA51, n=9). * p<0.05 vs EV; **** P ≤ 0.0001 vs EV.

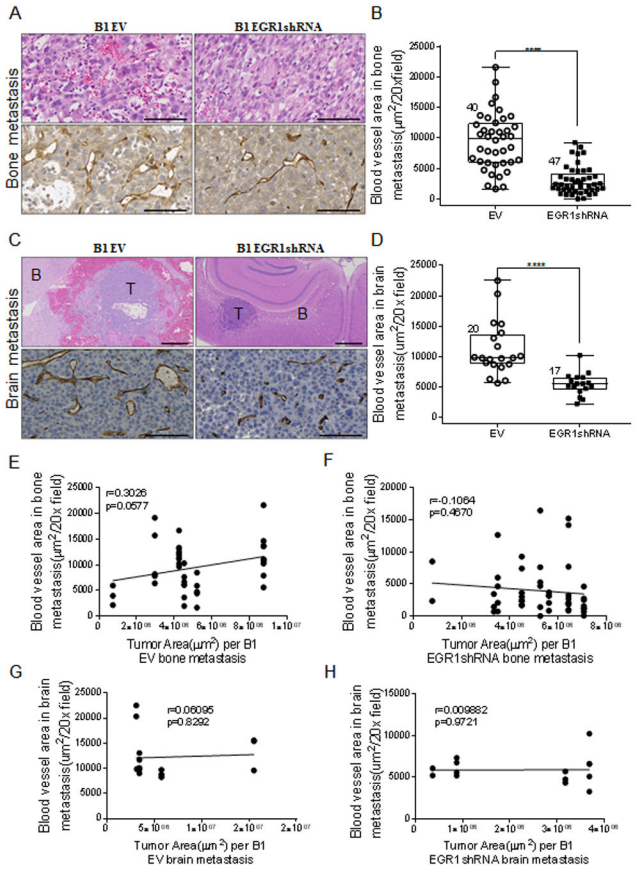

Figure 4. EGR1 depletion leads to decreased angiogenesis in prostate cancer bone and brain metastases.

(**A**) Representative histologic images depicting bone metastasis of mice bearing DU145 B1/ EV cells and DU145 B1/ EGR1shRNA tumors. Top panel: H&E, scale bar = 100 μm. Bottom panels: CD34 immunohistochemistry, scale bar = 100μm.

(**B**) Quantification of blood vessel density on CD34-stained sections of bone metastases. ****, P < 0.0001. 6 tumors were analyzed in EV group. 8 tumors were analyzed in EGR1shRNA group. Data points represent individual fields of view.

(**C**) Representative histologic images depicting brain metastasis of mice bearing DU145 B1/ EV and DU145 B1/ EGR1shRNA tumors. Top panel: H&E, scale bar = 500 μm. Bottom panels: CD34 immunohistochemistry, scale bar = 100μm. T, tumor; B, brain.

(**D**) Quantification of blood vessel density on CD34-stained sections of brain metastases. ****, P < 0.0001. 5 tumors were analyzed in each group. Data points represent individual fields of view.

(**E**) Correlation study between CD34-stained blood vessel density and tumor area in DU145 B1/ EV bone metastases (n=6). Pearson correlation test.

(**F**) Correlation study between CD34-stained blood vessel density and tumor area in DU145 B1/ EGR1shRNA bone metastases (n=8). Pearson correlation test.

(**G**) Correlation study between CD34-stained blood vessel density and tumor area in DU145 B1/ EV brain metastases (n=5). Pearson correlation test.

(**H**) Correlation study between CD34-stained blood vessel density and tumor area in DU145 B1/ EGR1shRNA brain metastases (n=4). Pearson correlation test.

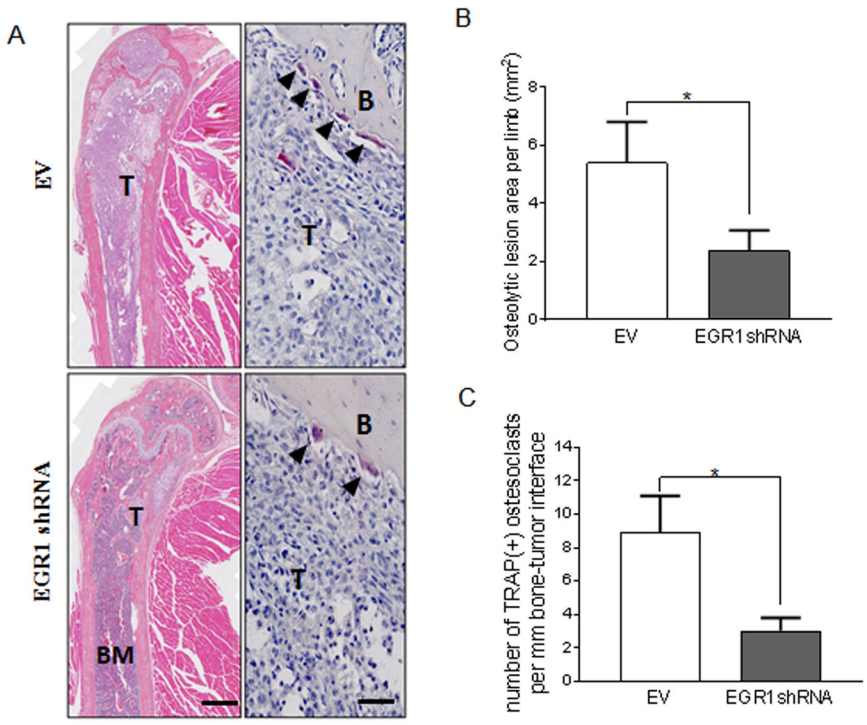

Figure 5. EGR1 depletion leads to reduced osteoclastogenesis in prostate cancer bone metastasis.

(**A**) Representative H&E (left) and TRAP staining images (right) from mice bearing DU145 B1/ EV or DU145 B1/ EGR1shRNA bone metastasis. Arrow heads indicate TRAP (+) osteoclasts. T, tumor; B, bone; BM, bone marrow. H&E staining, scale bar, 500 μm. TRAP staining, scale bar, 100μm.

(**B**) Quantification of osteolytic lesion area per limb. EV: n=28 limbs; EGR1shRNA: n=48 limbs; *, P<0.05.

(**C**) Quantification of TRAP (+) osteoclasts along the bone-tumor interface of metastases from each experimental group. Six tumors were analyzed in EV group. Eight tumors were analyzed in EGR1shRNA group.

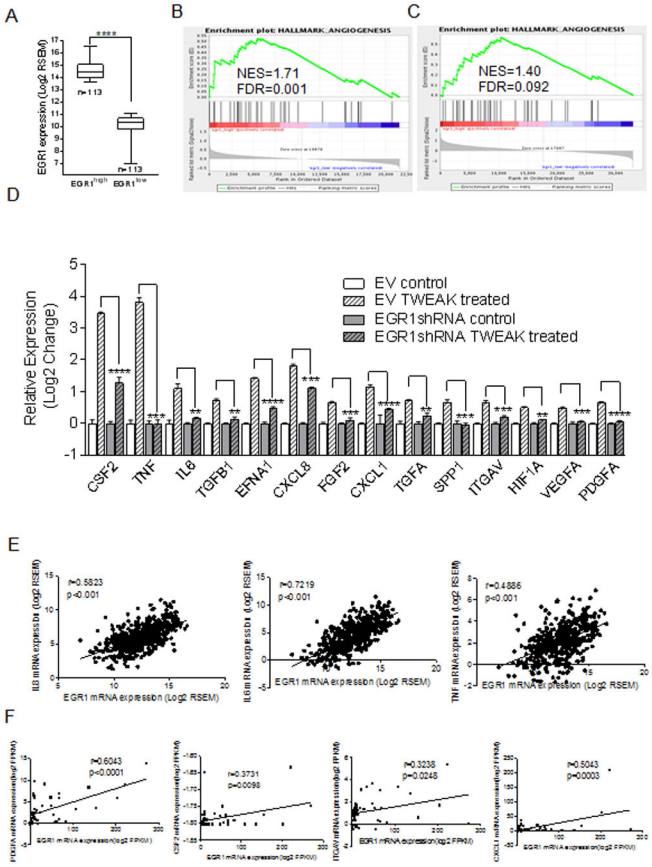

Figure 6. *EGR1* expression is required for select pro-angiogenic/osteoclastogenic factor expression in DU145 B1 cells and correlates with angiogenic/osteoclastogenic in clinical samples.

(**A**) Plots showing mean *EGR1* expression in the quartiles of patient samples with the highest (n=113) and with the lowest (n=113) levels in TCGA primary prostate cancer samples with Gleason score >7. ****, P < 0.0001.

(**B**) GSEA results showing significant [false discovery rate (i.e., FDR *q*-val) < 0.25] enrichment of angiogenesis genes comparing the two groups shown in Fig 6A.

(**C**) GSEA results showing significant [false discovery rate (i.e., FDR *q*-val) < 0.25] enrichment of angiogenesis genes comparing patient samples with the highest (n=10) and lowest (n=10) *EGR1* levels from the NEPC WCM 2016 mCRPC cohort.

(**D**) Osteoclastogenic and pro-angiogenic RNA levels in DU145 B1/ EV or DU145 B1/ EGR1shRNA11 cells with or without TWEAK (25ng/ml) for 2hr. **, P<0.01; ***, P<0.001, ****, P < 0.0001.

(**E**) Correlation plots between *EGR1* and RNA encoding select pro-angiogenic/ osteoclastogenic factors for all TCGA samples with GS>7 (Pearson correlation test).

(**F**) Correlation plots between *EGR1* and RNA encoding select pro-angiogenic/ osteoclastogenic factors for all samples in the NEPC WCM 2016 mCRPC cohort (Pearson correlation test).

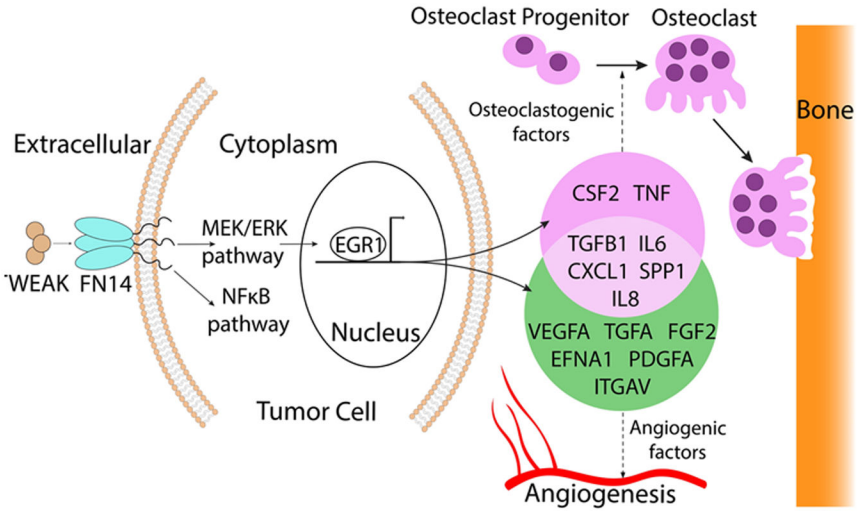

Figure 7.

Proposed model for EGR1-dependent genes contributing to angiogenesis/osteoclastogenesis in prostate cancer metastases.